Acta Materialia 127 (2017) 332–340

Contents lists available at ScienceDirect

Acta Materialia

journal homepage: www.elsevier.com/locate/actamat

Full length article

Statistical analysis of the size- and rate-dependence of yield and plastic flow in nanocrystalline copper pillars

Jung-A Lee [a], Moo-Young Seok [a], Yakai Zhao [a], In-Chul Choi [b], Dong-Hyun Lee [a], Brandon B. Seo [c], Upadrasta Ramamurty [d], Ting Y. Tsui [c, **], Jae-il Jang [a, *]

[a] Division of Materials Science and Engineering, Hanyang University, Seoul, 04763, Republic of Korea
[b] Institute for Applied Materials, Karlsruhe Institute of Technology, Karlsruhe, 76021, Germany
[c] Department of Mechanical Engineering, University of Waterloo, Waterloo, ON, N21 3G1, Canada
[d] Department of Materials Engineering, Indian Institute of Science, Bangalore, 560012, India

ARTICLE INFO

Article history:
Received 13 November 2016
Received in revised form
15 January 2017
Accepted 17 January 2017
Available online 18 January 2017

Keywords:
Nanocrystalline Cu
Micro-compression test
Statistical analysis
Size effect
Strain-rate sensitivity

ABSTRACT

The effects of specimen size and strain rate on the plastic deformation response of sub-μm-sized nanocrystalline Cu pillars were examined through a series of micro-compression experiments, with particular emphasis on the stochastic nature of the measured responses. A large number of micropillars two different diameters, both with an average grain size of 6 nm, were prepared by employing the single batch process of e-beam lithography and electroplating and tested. By recourse to statistical analysis, it was recognized the yield strength and flow stress increase with pillar size and strain rate. Further, the rate sensitivity in smaller pillars was more pronounced, implying synergetic interactions between the deformed volume and the strain rate imposed. The coupling influence of size and rate on yield was analyzed by estimating the parameters in a statistical distribution having Weibull-like formula, revealing that the enhanced role of free surface in smaller pillar may make it easy to trigger yielding. The size-dependence of rate-sensitive plastic flow was also statistically examined in detail and discussed in terms of strain-rate sensitivity, activation volume, and the combined roles of free surfaces and grain boundaries.

1. Introduction

The strain-rate sensitivity (SRS) of plastic deformation in metals and alloys is an extensively researched topic, as it is essential not only for better understanding of thermally activated processes, but also for developing improved manufacturing processes such as metal forming, high-speed machining, and other dynamic processes. This is accomplished by examining the mechanical properties of the material under investigation over a wide range of strain rates, $\dot{\varepsilon}$, and SRS is expressed in terms of the parameter m which is given by $\left(\frac{\partial \ln \sigma}{\partial \ln \dot{\varepsilon}}\right)_{\varepsilon,T}$ where σ is the flow stress. The published literature suggests that m is both the intrinsic length scales such as the grain size as well as extrinsic parameters such as the experimentally variable size of the specimen. For example, an increase in m with decreasing average grain size, d, has long been observed in face-centered cubic (fcc) metals [1–6]. This trend extends even to nanocrystalline (nc) metals (with d < 100 nm) of which m values are now known as ~0.01–0.03 [2–7]. This enhancement was attributed the increased role of grain boundaries (GBs) in the plastic deformation with decreasing d [3,4]. Likewise, the dependence of m on the sample diameter, D, – higher m for a smaller D–is attributed to the enhanced contribution of free surface [8–10]. Then, it is reasonable to expect that considerable enhancement in m could occur when micro-/nano-pillars having nano-sized grains are tested. This aspect remains unexplored hitherto. Further, only limited efforts have been made for investigating the possible synergetic effects of intrinsic and extrinsic size effects on the rate dependence of deformation (i.e., for the pillars having both D < 1 μm and d < 100 nm). A previous work by Zhang et al. [9,10] reported relatively high m (~0.18) of poly-crystal Cu pillars with D~500 nm. However, their pillars had relatively larger d (110 and 180 nm). Recent works by Mohanty et al. [11] and Wehrs

* Corresponding author.
** Corresponding author.
E-mail addresses: tttsui@uwaterloo.ca (T.Y. Tsui), jijang@hanyang.ac.kr (J.-i. Jang).

http://dx.doi.org/10.1016/j.actamat.2017.01.033
1359-6454/

et al. [12] explored the *m* of nc Ni pillars with $d < 30$ nm. However, these studies do not complete the picture as only size pillars (*D* larger than 1.5 μm) was utilized in both the studies [11,12]. We [13] have also reported the *m* of nc Ni pillars (with *d*~12 nm), but still the used pillars had single *D* of 1 μm. Therefore, better understanding of the synergetic effects of both intrinsic and extrinsic sizes on the rate-dependent deformation becomes the first motive of this study.

The second motive of this study, which is perhaps relatively more important, is related to the stochastic nature of the mechanical responses measured on small-volume sample, which is imparted by the smaller number of grains in combination with the finite number of dislocation sources at the very small scale (for example, see recent review [14]). Such inevitable stochastic behavior in the analysis of the size effects on the rate-dependent deformation is, hitherto, one of the issues remaining unsolved in the literature on the micro-compression experiments of small-sized pillars. To examine this, statistical analysis of the large data is essential. However, in most of the studies, which are concerned with plasticity, only limited number of the pillars were probed, e.g., only three pillars were tested for each condition in Refs. [11,12]. In prior studies, the tested pillars were usually prepared by focused ion beam (FIB) milling, which requires long time and hence is costly. Therefore, it is economically-unviable to conduct statistically significant number of micro-compression experiments on FIB-prepared pillars. For this reason, among a variety of nano-mechanical tests, nanoindentation test has been the most popularly used for statistical analysis of the strength fluctuations (using hardness and pop-in stress data [14–22]) thanks to its merits such as simple testing procedure and easy sample preparation.

Keeping the above factors in mind, we explored the stochastic nature of size effects on the rate-sensitive deformation of sub-μm-sized nc Cu pillars (having both $d < 10$ nm and $D \leq 1$ μm) through a series of micro-compression experiments under three different $\dot{\varepsilon}$. More than ~380 pillars (with *d*~7 nm, and *D*~550 and ~1000 nm) were prepared by a single batch process of e-beam lithography and electroplating. This fabrication technique offers several advantages: First is the high throughput with the possibility of simultaneous manufacturing hundreds of pillars. Second, the produced pillars are free from any surface damage that is typically attributed to FIB milling process [23]. Last, but not the least, strong sample uniformity across each substrate can be obtained through this fabrication method. From the statistical analysis of the results, the coupled influences of both size and rate on the yielding and plastic flow of the sub-μm-sized nc pillars were discussed in terms of statistical parameters, strain-rate sensitivity, activation volume, and combined roles of free surfaces and GBs.

2. Experimental

The nc Cu pillars examined in this work were fabricated via electron beam lithography and electroplating methods [23] as following. First, the silicon substrates covered with thin Ti (~25 nm) and Au (~25 nm) seed layers were spin coated with a polymethylmethacrylate (PMMA) resist. Subsequently, arrays of circular via-holes with diameters, *D,* of ~550 and ~1000 nm were patterned in the PMMA film using electron beam lithography. Next, these patterned molds were filled with nc Cu by electroplating by using a commercial grade pure Cu as anode. The solution was made of sulfuric acid, Cu (II) sulfate pentahydrate, thiourea, and ultra-pure water. After electroplating, the remaining PMMA resist was removed with acetone, so as to obtain pillar arrays.

Quasi-static micro-compression tests were performed on the pillars at room temperature (RT) using Nanoindenter XP (formerly MTS; now Keysight Tech., Oak Ridge, TN) with a FIB-milled cylindrical diamond punch having a top diameter of ~8 μm. During the tests, the pillars were loaded with nominal strain rates, $\dot{\varepsilon}$, ranging from 0.0002 to 0.005/s. The morphologies of pillars were imaged before and after the micro-compression tests through scanning electron microscopy (SEM) with Nova NanoSEM 450 (FEI Inc., Hillsboro, OR). Additionally, *in-situ* micro-compression tests were performed on pillars inside a Quanta 250 FEG SEM (FEI Inc., Hillsboro, OR) using a PI 85 picoindenter (Hysitron Inc., Mineapolis, MN). The microstructure of the pillars was examined with the aid of

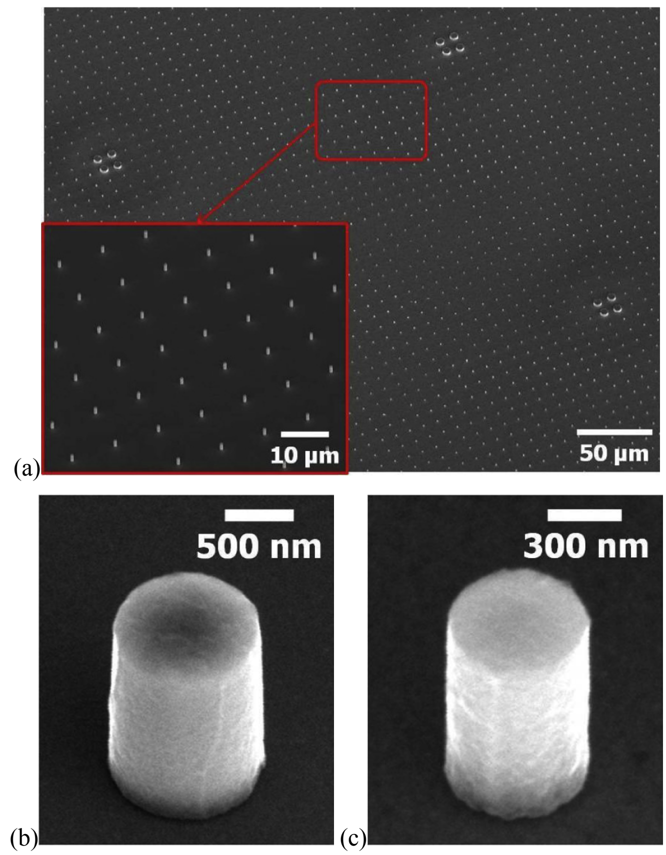

Fig. 1. Representative SEM images of prepared sample geometry; (a) electroplated pillar array; (b) morphology of as-fabricated pillar with *D* of ~1000 nm and (c) of ~550 nm.

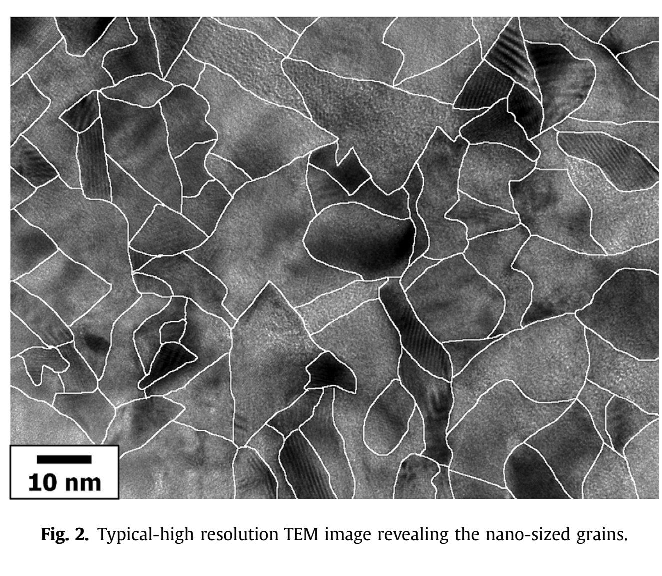

Fig. 2. Typical-high resolution TEM image revealing the nano-sized grains.

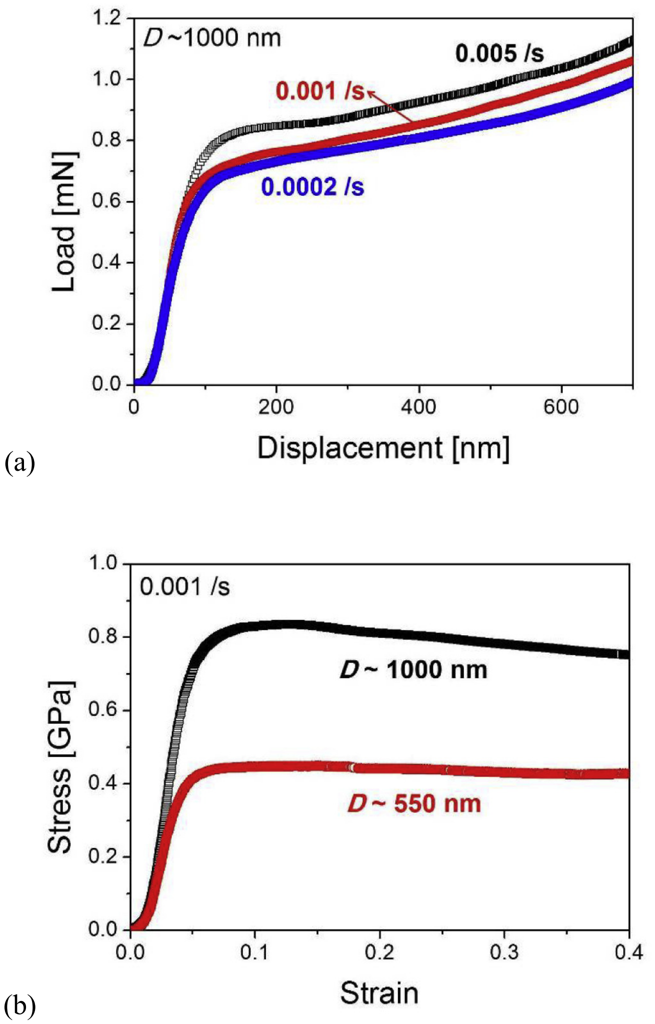

Fig. 3. Representative examples of (a) load-displacement curves (for D~1000 nm) and (b) true stress-true strain curves converted from load-displacement curves (for $\dot{\varepsilon}$ ~ 0.001/s).

transmission electron microscopy (TEM) with JEM-2010F (JEOL Ltd., Tokyo, Japan).

3. Results

3.1. Micro-compression tests

Fig. 1 shows the arrays and morphologies of as-fabricated nc Cu pillars. As already mentioned, a particular advantage of the applied fabrication method is high throughput with hundreds of uniformly spaced pillars on one substrate, which is clearly seen through Fig. 1(a). An additional advantage is that the top surfaces of the pillars are flat while the side-surfaces are almost taper-free, as seen from Fig. 1(b) and (c) that display higher magnification images of the pillars with the nominal outer diameter D of ~1000 and ~550 nm and aspect ratios of are ~1.4 and ~1.5 respectively. A high-resolution TEM image obtained from a pillar with D~1000 nm is displayed in Fig. 2. From such images, the grain size, d, of the pillars was determined to be ~6 nm, which was measured using multiple TEM micrographs taken at various locations on each pillar.

Typical examples of load-displacement (P-h) curves that were recorded during micro-compression tests are provided in Fig. 3(a). From the P–h data, true stress (σ) vs. true strain (ε) curves were extracted with general assumptions of volume conservation ($A_0L_0 = A_pL_p$ where A and L are cross-sectional area and height of pillar, respectively, whereas subscripts "0" and "p" indicate "initial" and "during plastic deformation," respectively). In Fig. 3(b), representative σ-ε curves for both D~1000 and ~550 nm obtained at $\dot{\varepsilon}$ of 0.001/s are compared. It is seen that the plastic flow resistance of the larger diameter pillars (D~1000 nm) is considerably higher than those with smaller D (~550 nm). Similar "smaller is weaker" behavior was previously reported for the pillars of nc fcc metals such as nc Cu [24,25], Ni-W [26], Ni [27], and Pt [28].

Fig. 4 shows representative SEM images of the ~1000 and ~550 nm diameter pillars taken before and after micro-compression tests. In both the cases, large plasticity was observed, i.e., the pillars could be deformed until they become pancake-shaped. This interesting superplastic-like deformation at relatively high $\dot{\varepsilon}$ (10^{-3}–10^{-1}/s) and at RT was also reported for nc Ni

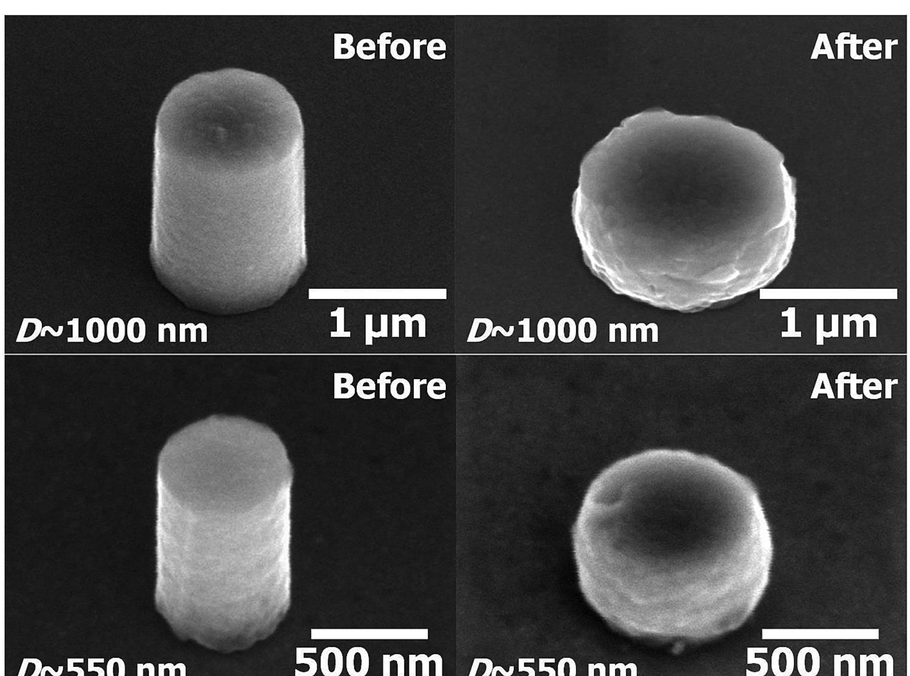

Fig. 4. SEM images taken before and after the micro-compression tests (for $\dot{\varepsilon}$ ~ 0.005/s).

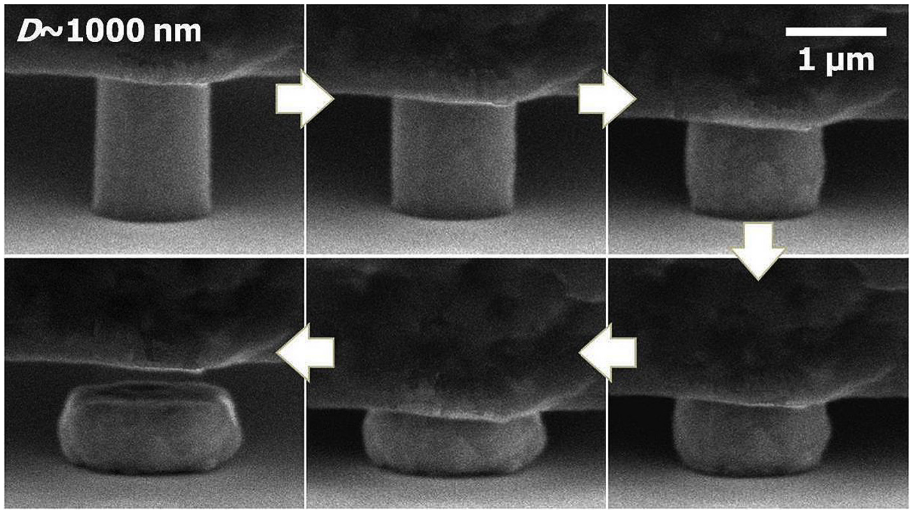

Fig. 5. Snap shots taken during *in-situ* micro-compression test (for $\dot{\varepsilon}$ ~ 0.005/s).

previously [13,29]. To directly visualize the deformation, *in-situ* micro-compression tests were performed on the pillars for *D*~1000 nm. The captured video frames are provided in Fig. 5. During loading, the deformation was found to be uniform with neither a sudden geometry change nor localization of failure.

3.2. Statistical inference

We have conducted more than 60 tests for each condition, so as to conduct a critical statistical examination of the mechanical behavior of the micropillars. The *P*-*h* data for a large number of tests, displayed in Fig. 6, illustrates the disperse nature of the measured mechanical responses and justifies a detailed statistical analysis. For this, both yield strength, σ_y, and flow stress, σ_f, were analyzed to investigate their dependence on *D* and $\dot{\varepsilon}$. Since the determination of the exact value of σ_y is difficult due to a continuous transition from elastic to elasto-plastic deformation regimes of the stress-strain response, flow stress obtained by a strain offset of 1%, was designated as σ_y (see Fig. 7). Additionally, σ_f at various remnant plastic strain, ε_p, values where ε_p is the amount of remaining ε after unloading, i.e., the total strain minus elastic strain, ε_e, as illustrated in Fig. 7.

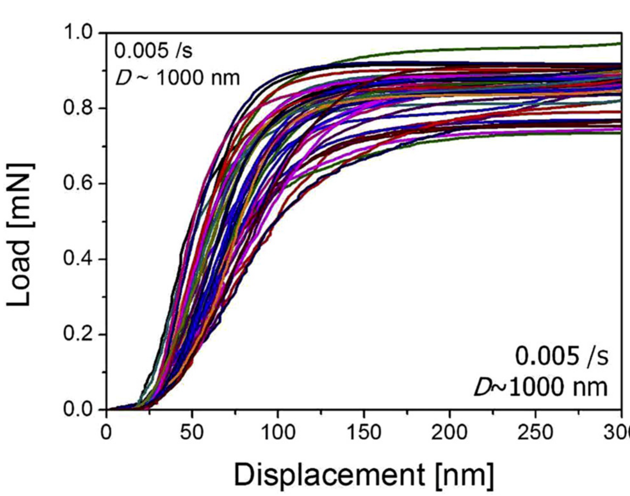

Fig. 6. The data set of *P*-*h* curves for *D*~1000 nm and $\dot{\varepsilon}$ ~ 0.005/s.

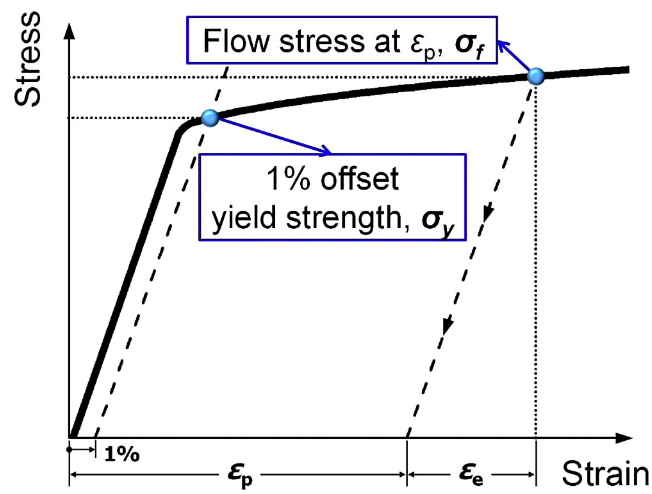

Fig. 7. Schematic illustration showing how to determine σ_y and σ_f.

The dispersions in σ_y and σ_f (for $\varepsilon_p = 0.1$, for instance) for the two different *D* examined in this study are illustrated through histograms (whose bin sizes are 0.025 GPa for *D*~1000 nm and 0.05 GPa for *D*~550 nm) in Figs. 8 and 9, respectively. We approximate these distributions to be Gaussian in nature; the continuous distributions (estimated by using the mean and standard deviations) are drawn as solid lines on these histograms. Two trends are noteworthy. First, in all the cases, the mean value increases with $\dot{\varepsilon}$, which is pronounced for *D*~550 nm. Second, the distribution obtained at $\dot{\varepsilon} = 0.005$/s is much wider as compared to the others obtained at different $\dot{\varepsilon}$. We also observe that the dispersion gets wider with increasing $\dot{\varepsilon}$.

For further analysis of the observed trends, statistical inference was obtained by using a two-way analysis of variance (ANOVA) [30,31]. It enables us to assess not only the effect of each independent experimental variable (i.e., *D* and $\dot{\varepsilon}$ in this study) on the overall dispersion, but also the synergy between them, if any. Details of the analysis procedure adapted are provided elsewhere [30,31]. The results of such an analysis for σ_y and σ_f are summarized in Table 1 from which, it is clear that the interaction between each source (*D* and $\dot{\varepsilon}$) is statistically significant; i.e., the *p*-value is very close to zero. This suggests that the rate sensitivity depends on the

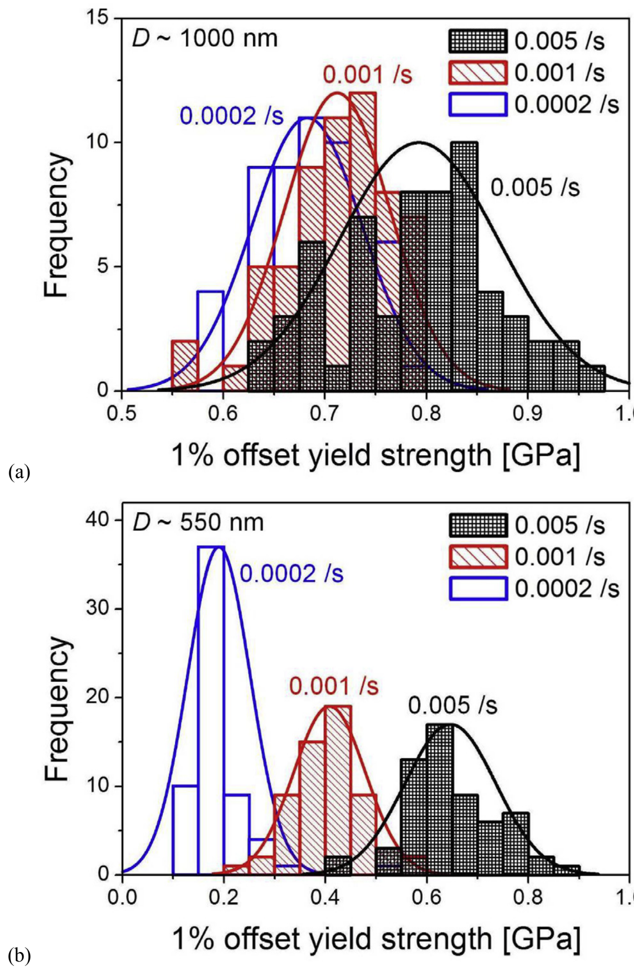

Fig. 8. Histograms and Gaussian distributions of σ_y for pillars with (a) D~1000 and (b) D~550 nm.

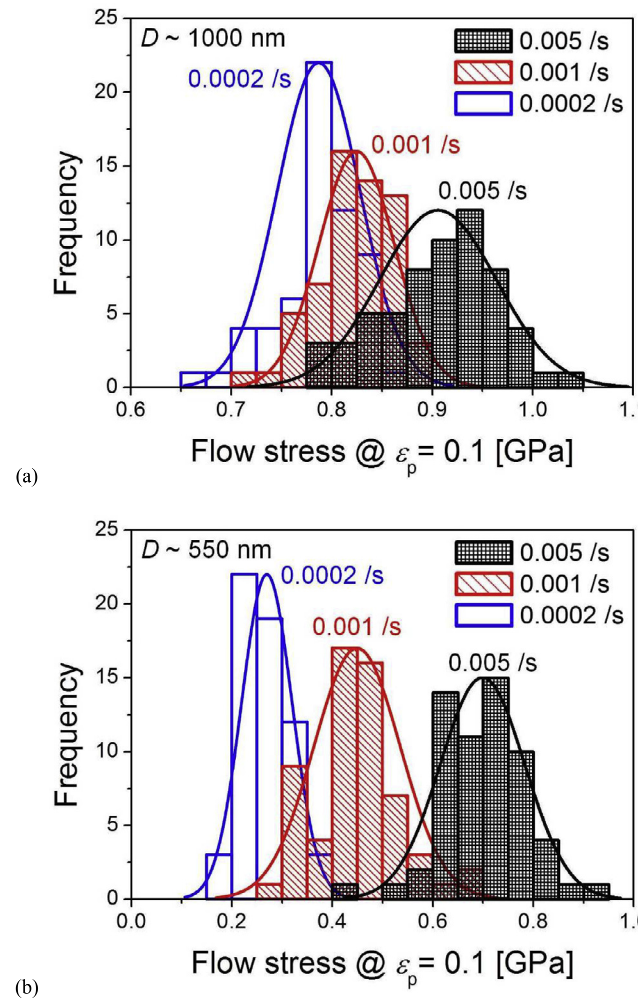

Fig. 9. Histograms and Gaussian distributions of σ_f at $\varepsilon_p = 0.1$ for pillars with (a) D~1000 and (b) D~550 nm.

pillar diameter; i.e., smaller the pillar, more pronounced it is to the imposed rate of deformation.

Although some inferences can be drawn from the above analysis, it is insufficient to ascertain whether or not one pair (or group) of mean values for a specific set of experimental conditions (especially, for $\dot{\varepsilon}$) is significantly different from others. Here, since three different $\dot{\varepsilon}$ (0.0002, 0.001, and 0.005/s) were utilized, it is necessary to check the validity of the influence at each level (i.e., between 0.0002 and 0.001/s and between 0.001 and 0.005/s) independently, which cannot be examined by two-way ANOVA. Thus, for each D, we additionally performed one-way ANOVA, followed by Tukey's test for the post-hoc analysis [30,31]. The results reveal that both σ_y and σ_f increase significantly within the $\dot{\varepsilon}$ ranges of 0.0002–0.001 and 0.001–0.005/s. Specifically, the mean difference obtained from Tukey's test is larger for D ~550 nm than that for D ~1000 nm, which indicates to a more obvious $\dot{\varepsilon}$ dependency of the former. A comparison of the mean differences suggested that a lower $\dot{\varepsilon}$ can lead to more pronounced reduction in σ_y and σ_f with decreasing D. These trends are graphically summarized in Fig. 10.

4. Size-dependence of rate sensitivity

4.1. Yield strength

Rate dependency of plastic deformation in small volumes of single- as well as poly-crystal materials has been investigated in a number of recent studies [8–12,32]. Zhu et al.'s simulation work on Cu nanowires [32] suggests that the rate-sensitive yielding in a small volume of material is governed by the nucleation of dislocations at the free surfaces. On this basis, an analytical expression for the dislocation nucleation stress (σ_n) was derived as [32];

$$\sigma_n = \sigma_a - \frac{kT}{V^*} \ln \frac{kTN\nu}{E\dot{\varepsilon}V^*} \tag{1}$$

where σ_a is the athermal stress associated with the dislocation nucleation, V^* is the activation volume, k is Boltzmann constant, T is the absolute temperature, N is the number of nucleation sites available, ν is the attempt frequency, and E is Young's modulus. This equation provides a basis for the understanding of some of the results of the present study. First, σ_n is dependent not only on T and $\dot{\varepsilon}$ but also on N, which implies a size effect as smaller pillars will necessarily mean smaller N. Second, in the equation, the term (kT/V^*) pre-multiplies the logarithm. Thus, at a given T and N, smaller V^* results in higher rate sensitivity of σ_n.

Table 1
Two-way ANOVA results for "interaction" of D and $\dot{\varepsilon}$.

	Degree of freedom	Sum of squares	Mean squares	*F*-value	*p*-value
For σ_y	2	1.852	0.926	208.1	1.8E-60
For σ_f	2	1.449	0.724	183.8	1.8E-55

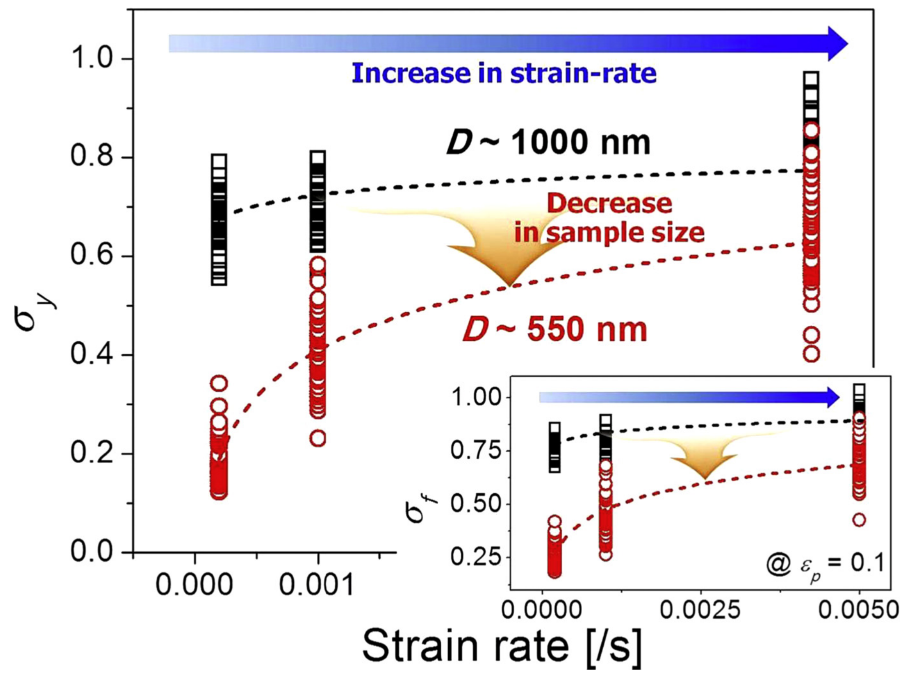

Fig. 10. Summary of the variation in σ_y for pillars as a function of $\dot{\varepsilon}$ and the inset image show the variation in σ_f at $\varepsilon_p = 0.1$.

An interesting observation made in Zhu et al.'s study [32] is that the V^* associated with the surface dislocation nucleation is in the range of ~1–10b^3 (where b is the Burgers vector) which is much lower than that of a dislocation in the bulk and is close to that for diffusion process. Recently, Chen et al. [33] also reported that surface dislocation nucleation requires a small V^*, which is similar to that for diffusion process. From these studies, it is reasonable to assume that the size-dependence of rate-sensitive yielding observed in the present study is also related to surface diffusion and dislocation nucleation.

The cumulative probability for yielding, f, and V^* are often related through the following equation [15,16]:

$$f = 1 - \exp\left[-\frac{kT\dot{\gamma}_0}{V^*(\mathrm{d}\tau/\mathrm{d}t)} \exp\left(-\frac{\Delta F^*}{kT} \right) \exp\left(\frac{\tau V^*}{kT} \right) \right] \quad (2)$$

The above equation can be rewritten as

$$V^* = kT \frac{\partial \ln\left[\ln(1-f)^{-1}\right]}{\partial \tau} = \sqrt{3}kT \frac{\partial \ln\left[\ln(1-f)^{-1}\right]}{\partial \sigma_y}. \quad (3)$$

Although V^* can capture the effects of T and $\dot{\varepsilon}$ on the strength variation, it cannot capture their possible influences on the strength distribution. It is important to recognize that the potential dislocation source at nanoscale is intrinsically stochastic in nature. Therefore, a dispersion in the measured σ_y would be natural (see Fig. 8). In this regard, some efforts to use the Weibull distribution for statistical analysis of the nanomechanical measurements (i.e., jerky flow and size effect in micro-compression results [34–38]) were made, although the Weibull distribution is typically used for analyzing the fracture strength of brittle materials [39–41]. For yielding, the applied formula of Weibull distribution is typically given by,

$$f = 1 - \exp\left[-V \left(\frac{\sigma_y}{\sigma_0} \right)^{\omega} \right] \quad (4)$$

where V is volume, ω is the shape parameter (or Weibull modulus), and σ_0 is the scale parameter. Equation (4) suggests that a larger V corresponds to a higher probability for yielding, indicating that the weakest-link scaling of strength implicitly assumed in Weibull statistics imparts a size effect automatically [39,40]. In this study, however, the observed size effect is opposite to this expectation, i.e., the smaller pillar has lower σ_y. As elaborated above, the weakening mechanism is conceivably associated with increased fraction of free surface in a smaller pillar. This observation implies that it may be more apt to replace V in Eq. (4) with the surface-to-volume ratio (SVR), S/V where S is surface area:

$$f = 1 - \exp\left[-\left(\frac{S}{V} \right)^{\alpha} \left(\frac{\sigma_y}{\sigma_0} \right)^{\omega} \right] \quad (5)$$

where α is the SVR-dependent exponent. Note that although there is a mathematical similarity, Eq. (5) cannot be called a real Weibull distribution formula because the physical meaning for the influence of SVR on yield strength can be against the weakest-link theory. Since a higher value of (S/V) in a smaller pillar results in higher f for yielding, this equation may be appropriate to explain the yielding behavior of nc Cu pillars examined here. In this "Weibull-like" formula, the shape parameter, ω, can reflect not only the strength variability but also the magnitude of activation volume V^*. The value of ω can be simply expressed by

$$\omega = \frac{\partial \ln\left[\ln(1-f)^{-1}\right]}{\partial \ln \sigma_y}. \quad (6)$$

By integrating Eqs. (3) and (6), one can readily show

$$\omega = \frac{\sigma_y V^*}{\sqrt{3}kT}. \quad (7)$$

Since ω is proportional to V^*, it can be deduced that ω may play a similar role to that of V^* in Eq. (1); i.e., a lower ω (thus, lower V^*) can bring out the enhancement of rate-sensitive deformation. The SVR-dependent exponent, α, is an indicator for the probed material's sensitivity to SVR; e.g., if α is zero or close to zero, the material's yield response is size-insensitive. The value of α can be estimated from the relation between mean strength, $\overline{\sigma}_y$, and (S/V):

$$\overline{\sigma}_y = \sigma_0 \Gamma\left(1+\frac{1}{\omega}\right)\left(\frac{S}{V}\right)^{-\alpha/\omega}. \tag{8}$$

where $\sigma_0\Gamma\left(1+\frac{1}{\omega}\right)$ is constant, and $\Gamma\left(1+\frac{1}{\omega}\right)$ is a gamma function. The $-\alpha/\omega$ values can be obtained from the slope of the linear plot of $\ln(S/V)$ and $\ln\overline{\sigma}_y$, and then the value of α for each condition can be determined by dividing into ω.

Based on Eqs. (6) and (8), the best fits for the datasets of σ_y are provided in Fig. 11 where estimated ω and α are also given. When D is reduced from ~1000 to ~550 nm, the SVR increases from 0.0046 to 0.0082/nm and the ω value decreases from ~11–16 to ~6–9, suggesting that the increased fraction of the surfaces results in a wider distribution of the yield strength. More importantly, it reveals that a smaller pillar exhibits a lower activation volume and thus a higher rate sensitivity. In turn, it provides a plausible explanation that in a smaller pillar, the enhanced role of the surface nucleation may make it easy to trigger yielding at lower stresses and clearly manifest the rate sensitivity. In addition, extremely high value of α (~4–25) and a significant change with $\dot{\varepsilon}$ support that the SVR markedly affect the rate-sensitive deformation and its mechanism.

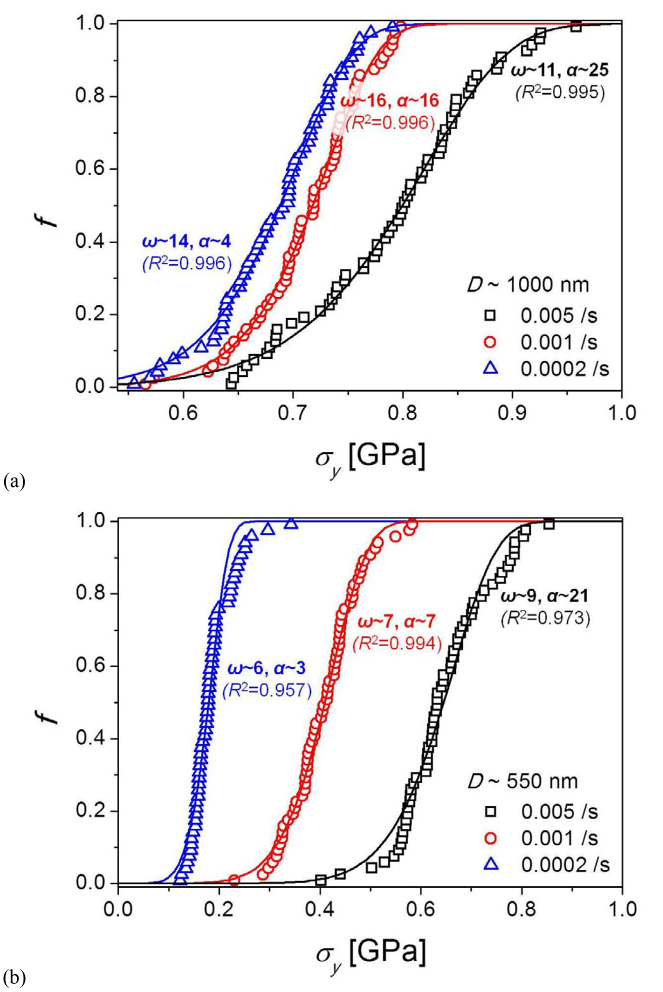

Fig. 11. Weibull plots for yield strength of nc Cu pillars with the parameters of ω and α; (a) D~1000 and (b) D~550 nm.

4.2. Flow stress

To explore the plastic deformation mechanism beyond yield, we examined strain-rate sensitivity in the plastic flow regime, m, which is determined by relating σ_f and $\dot{\varepsilon}$ through

$$\sigma_f = K\dot{\varepsilon}^m \tag{9}$$

where K is a correlation constant. As a representative example, the plot of σ_f (at ε_p of 0.1) vs. $\dot{\varepsilon}$ is given in the inset image of Fig. 12(a) where m is 0.042 and 0.29 for D~1000 and ~550 nm, respectively. The values of m are summarized as a function of ε_p in Fig. 12(a); note that m for D ~550 nm is ~7–8 times higher than that for D~1000 nm.

Rate sensitivity of deformation in nc metals is through to be a result of the high GB fraction in them [2–7]. For an fcc metal, the relation between m and d is given as [5]

$$m = \frac{kT}{\xi b}\frac{1}{\chi\left(\alpha\sqrt{\rho d}+\beta\sqrt{d}\right)}. \tag{10}$$

Here, ξ, α, and β are proportionality factors, χ is the unit distance that is swept by a mobile dislocation and is approximately constant on the order of b, and ρ is the dislocation density (which can be

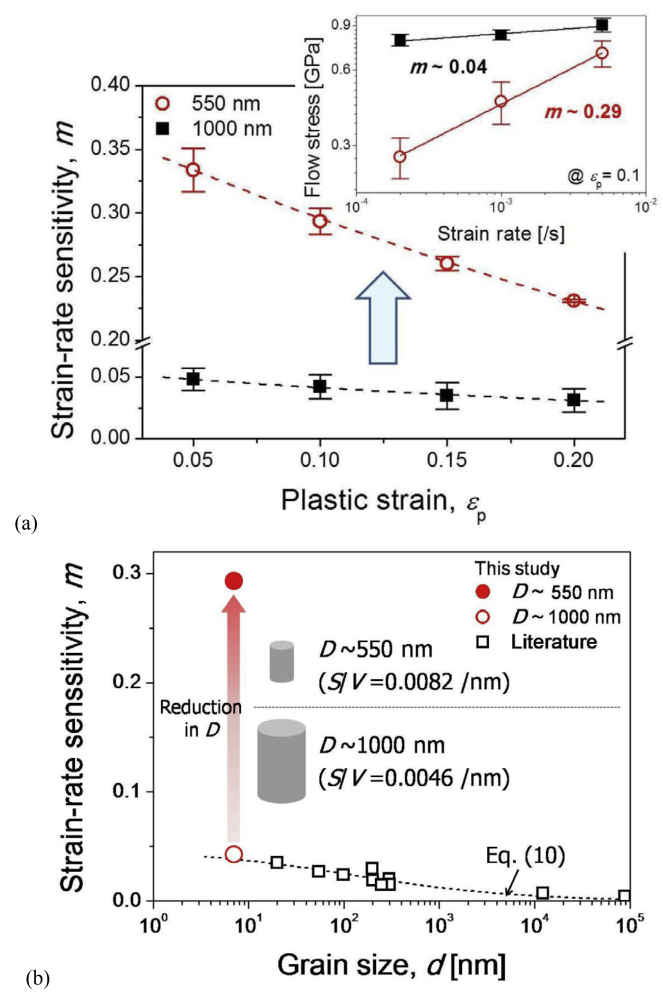

Fig. 12. Variations in m (a) as a function of ε_p with the inset showing how to estimate m (for ε_p = 0.1), and (b) as a function of d for Cu using experimental data from the literature [1,4,43,44] and from the present work.

correlated with ε_p by Orowan equation $\rho = \varepsilon_p/(b\lambda)$ where λ is the mean free path of dislocation slip [42]). Representative m values for Cu bulk samples reported in the literature [1,4,43,44] along with those obtained in the present study are plotted in Fig. 12(b). The best fit of Eq. (10) through the entire data is also plotted. The m for D~1000 nm appears to be in a good agreement with that predicted using Eq. (10), implying that the nature of the plasticity in the pillars with D ~1000 nm is similar to those of bulk samples. In the case of D ~550 nm, however, the m value is much higher than the value expected from Eq. (10). This indicates that the pillar size itself (if it is smaller than a critical value) can markedly affect the plastic deformation of nc metals independent of microstructural effects such as effects of d.

The procedure for the estimation of V^* associated with the plastic flow is generally different from that used for yielding [i.e., based on Eq. (3)] since it is less stochastic in nature. From its definition, it can be simply determined by:

$$V^* = \sqrt{3}kT\left(\frac{\partial \ln\dot{\varepsilon}}{\partial \sigma_f}\right) \quad (11)$$

The estimated values of V^* at various ε_p are shown in Fig. 13(a). Of that, σ_f at ε_p of 0.1 as a function of $\dot{\varepsilon}$ is plotted in the inset image. The

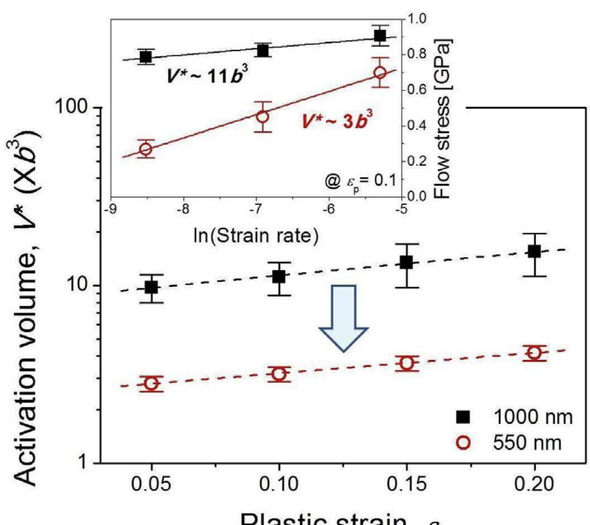

(a)

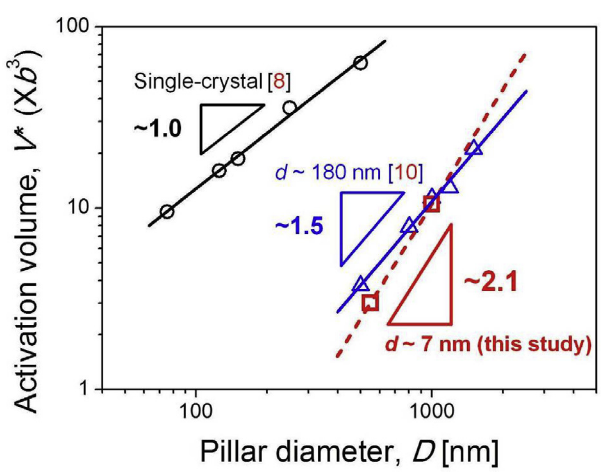

(b)

Fig. 13. Variations in activation volume, V^*; (a) V^* vs. ε_p (with inset showing an example of how to determine V^*, for $\varepsilon_p = 0.1$); (b) V^* vs. D relations from this study and literature [8,10].

V^* for D ~1000 nm is ~$11b^3$ and for D~550 nm is ~$3b^3$.

To better understand the influence of the pillar size on the rate sensitivity of plastic deformation, V^* obtained in the present work are plotted along those reported in literature [8,10] as a function of D in Fig. 13(b) where literature Cu data for single-crystal [8] and d~180 nm [10] are also given. For both poly-and single-crystal cases, a linear relation between V^* and D on a log-log scale is observed; i.e., V^* values decrease significantly with decreasing D. Although direct comparison of all the data plotted in this figure may not be accurate in view of the differences in applied $\dot{\varepsilon}$ as well as the ranges of ε over which they are obtained [8,10], a clear trend of a increase in the slope with a reduction in d (and thus increasing faction of GBs) can be noted. This observation implies that the size-dependency of V^* is more pronounced for a smaller d. On this basis, it is reasonable to conclude that a strong coupling between free surfaces and GBs (whose fractions are associated with D and d, respectively) influences the rate sensitivity of plasticity in micropillars. A possibility for this could be surface-enhanced GB-mediated deformation and/or high dislocation activities at surface/GB intersections. Both experimental and simulation works reported in literature [24,45–48] suggest that the GB-mediated deformation (including GB sliding and grain rotation which are directly related with superplasticity and high m in conventional fine-grained metals [49]) in the proximity of free surface occurs more easily than in the pillar interior, possibly due to the role of free surface as a relaxer of mechanical constraints [46]. In addition, such noticeable GB-mediated process near surface can lead to the formation of small surface steps/grooves on the order of atomic spacing at some of the GB/free surface intersections [25,50]. Such surface defects of the nanostructures can lower the activation barrier for plastic deformation due to local stress concentration, which is helpful for superplastic-like behavior. Thus, the pillar with larger fraction of GBs (that can lead larger fraction of potential stress concentration sites) may exhibit a noticeable rate-sensitive deformation than that with smaller fraction.

5. Conclusion

In the present study, the size-dependence of rate-sensitive deformation in nc Cu pillars having two different sizes was systematically investigated with a particular emphasis on the stochastic aspects of deformation. The influence of two experimental variables (D and $\dot{\varepsilon}$) on the yield as well as the plastic flow behavior was statistically analyzed. Results reveal that both σ_y and σ_f increase with D and $\dot{\varepsilon}$. Further, synergy between D and $\dot{\varepsilon}$ was noticed, i.e., the rate sensitivity in smaller pillars is more pronounced. This was discussed in terms of the estimated ω, α, and V^*. Increased contribution of free surface for smaller pillars results in a wider strength distribution and a lower activation volume, which can be indirectly evidenced by lower ω. The enhanced role of the surface nucleation can lead to an easier trigger of yielding and obvious rate-sensitive deformation in small pillars. Beyond yield, the assessment of m for plastic flow showed a considerably higher m in smaller pillars compared with nc bulk counterparts. In addition, the obtained V^* values were compared with those in the literature, leading to the trend that larger reduction in V^* with decreasing D is exhibited in a smaller d pillar. It can be rationalized in consideration of the enlarged contribution of free surface and the enhanced coupling with GBs.

Acknowledgement

The work at Hanyang University was supported in part by the National Research Foundation of Korea grant funded by the Korea government (MSIP) (No. NRF-2014M2A8A1030385), and in part by the NRF grant funded by the MSIP (No. NRF-2015R1A5A1037627).

References

[1] R.P. Carreker Jr., W.R. Hibbard Jr., Tensile deformation of high-purity copper as a function of temperature, strain rate, and grain size, Acta Metall. 1 (1953) 657–663, 654,655.
[2] F. Dalla Torre, H. Van Swygenhoven, M. Victoria, Nanocrystalline electrodeposited Ni: microstructure and tensile properties, Acta Mater. 50 (2002) 3957–3970.
[3] R. Schwaiger, B. Moser, M. Dao, N. Chollacoop, S. Suresh, Some critical experiments on the strain-rate sensitivity of nanocrystalline nickel, Acta Mater. 51 (2003) 5159–5172.
[4] Q. Wei, S. Cheng, K.T. Ramesh, E. Ma, Effect of nanocrystalline and ultrafine grain sizes on the strain rate sensitivity and activation volume: fcc versus bcc metals, Mater. Sci. Eng. A 381 (2004) 71–79.
[5] S. Cheng, E. Ma, Y.M. Wang, L.J. Kecskes, K.M. Youssef, C.C. Koch, U.P. Trociewitz, K. Han, Tensile properties of in situ consolidated nanocrystalline Cu, Acta Mater. 53 (2005) 1521–1533.
[6] J. Chen, L. Lu, K. Lu, Hardness and strain rate sensitivity of nanocrystalline Cu, Scr. Mater. 54 (2006) 1913–1918.
[7] Y.M. Wang, E. Ma, On the origin of ultrahigh cryogenic strength of nanocrystalline metals, Appl. Phys. Lett. 85 (2004) 2750–2752.
[8] A.T. Jennings, J. Li, J.R. Greer, Emergence of strain-rate sensitivity in Cu nanopillars: transition from dislocation multiplication to dislocation nucleation, Acta Mater. 59 (2011) 5627–5637.
[9] J.Y. Zhang, G. Liu, J. Sun, Strain rate effects on the mechanical response in multi- and single-crystalline Cu micropillars: grain boundary effects, Int. J. Plast. 50 (2013) 1–17.
[10] J.Y. Zhang, X. Liang, P. Zhang, K. Wu, G. Liu, J. Sun, Emergence of external size effects in the bulk-scale polycrystal to small-scale single-crystal transition: a maximum in the strength and strain-rate sensitivity of multicrystalline Cu micropillars, Acta Mater. 66 (2014) 302–316.
[11] G. Mohanty, J.M. Wheeler, R. Raghavan, J. Wehrs, M. Hasegawa, S. Mischler, L. Philippe, J. Michler, Elevated temperature, strain rate jump microcompression of nanocrystalline nickel, Phil. Mag. 95 (2015) 1878–1895.
[12] J. Wehrs, G. Mohanty, G. Guillonneau, A.A. Taylor, X. Maeder, D. Frey, L. Philippe, S. Mischler, J.M. Wheeler, J. Michler, Comparison of in situ micromechanical strain-rate sensitivity measurement techniques, JOM 67 (2015) 1684–1693.
[13] J.-A. Lee, B.B. Seo, I.-C. Choi, M.-Y. Seok, Y. Zhao, Z. Jahed, U. Ramamurty, T.Y. Tsui, J.-I. Jang, Time-dependent nanoscale plasticity in nanocrystalline nickel rods and tubes, Scr. Mater. 112 (2016) 79–82.
[14] Y. Gao, H. Bei, Strength statistics of single crystals and metallic glasses under small stressed volumes, Prog. Mater. Sci. 82 (2016) 118–150.
[15] C.A. Schuh, A.C. Lund, Application of nucleation theory to the rate dependence of incipient plasticity during nanoindentation, J. Mater. Res. 19 (2004) 2152–2158.
[16] C.A. Schuh, J.K. Mason, A.C. Lund, Quantitative insight into dislocation nucleation from high-temperature nanoindentation experiments, Nat. Mater. 4 (2005) 617–621.
[17] C.E. Packard, O. Franke, E.R. Homer, C.A. Schuh, Nanoscale strength distribution in amorphous versus crystalline metals, J. Mater. Res. 25 (2010) 2251–2263.
[18] H. Somekawa, C.A. Schuh, Effect of solid solution elements on nanoindentation hardness, rate dependence, and incipient plasticity in fine grained magnesium alloys, Acta Mater. 59 (2011) 7554–7563.
[19] I.-C. Choi, Y. Zhao, B.-G. Yoo, Y.-J. Kim, J.-Y. Suh, U. Ramamurty, J.-I. Jang, Estimation of the shear transformation zone size in a bulk metallic glass through statistical analysis of the first pop-in stresses during spherical nanoindentation, Scr. Mater. 66 (2012) 923–926.
[20] I.-C. Choi, Y. Zhao, Y.-J. Kim, B.-G. Yoo, J.-Y. Suh, U. Ramamurty, J.-i. Jang, Indentation size effect and shear transformation zone size in a bulk metallic glass in two different structural states, Acta Mater. 60 (2012) 6862–6868.
[21] Y. Zhao, I.-C. Choi, M.-S. Seok, M.-H. Kim, D.-H. Kim, U. Ramamurty, J.-Y. Suh, J.-I. Jang, Effect of hydrogen on the yielding behavior and shear transformation zone volume in metallic glass ribbons, Acta Mater. 78 (2014) 213–221.
[22] I.-C. Choi, D.-H. Lee, B. Ahn, K. Durst, M. Kawasaki, T.G. Langdon, J.-I. Jang, Enhancement of strain-rate sensitivity and shear yield strength of a magnesium alloy processed by high-pressure torsion, Scr. Mater. 94 (2015) 44–47.
[23] M.J. Burek, J.R. Greer, Fabrication and microstructure control of nanoscale mechanical testing specimens via electron beam lithography and electroplating, Nano Lett. 10 (2010) 69–76.
[24] N.L. Okamoto, D. Kashioka, T. Hirato, H. Inui, Specimen- and grain-size dependence of compression deformation behavior in nanocrystalline copper, Int. J. Plast. 56 (2014) 173–183.
[25] D.V. Badami, Z. Jahed, B.B. Seo, M.J. Burek, T.Y. Tsui, Microstructural and geometrical effects on the deformation behavior of sub-micron scale nanocrystalline copper pillars, Metall. Mater. Trans. A 47 (2016) 1061–1071.
[26] D. Jang, J.R. Greer, Size-induced weakening and grain boundary-assisted deformation in 60 nm grained Ni nanopillars, Scr. Mater. 64 (2011) 77–80.
[27] B.B. Seo, Z. Jahed, M.J. Burek, T.Y. Tsui, Influence of grain size on the strength size dependence exhibited by sub-micron scale nickel structures with complex cross-sectional geometries, Mater. Sci. Eng. A 596 (2014) 275–284.
[28] X.W. Gu, C.N. Loynachan, Z. Wu, Y.-W. Zhang, D.J. Srolovitz, J.R. Greer, Size-dependent deformation of nanocrystalline Pt nanopillars, Nano Lett. 12 (2012) 6385–6392.
[29] D. Pan, S. Kuwano, T. Fujita, M.W. Chen, Ultra-large room-temperature compressive plasticity of a nanocrystalline metal, Nano Lett. 7 (2007) 2108–2111.
[30] A.J. Hayter, Probability and Statistics for Engineers and Scientists, third ed., Duxbury Press, Belmont, 2006.
[31] R.L. Mason, R.F. Gunst, J.L. Hess, Statistical Design and Analysis of Experiments: with Applications to Engineering and Science, second ed., J. Wiley, New York, 2003.
[32] T. Zhu, J. Li, A. Samanta, A. Leach, K. Gall, Temperature and strain-rate dependence of surface dislocation nucleation, Phys. Rev. Lett. 100 (2008) 025502.
[33] L.Y. Chen, M.-R. He, J. Shin, G. Richter, D.S. Gianola, Measuring surface dislocation nucleation in defect-scarce nanostructures, Nat. Mater. 14 (2015) 707–713.
[34] A.H.W. Ngan, Size dependence and stochastic nature of yield strength of micron-sized crystals: a case study on Ni3Al, Proc. R. Soc. A-Math. Phys. Eng. Sci. 462 (2006) 1661–1681.
[35] T.A. Parthasarathy, S.I. Rao, D.M. Dimiduk, M.D. Uchic, D.R. Trinkle, Contribution to size effect of yield strength from the stochastics of dislocation source lengths in finite samples, Scr. Mater. 56 (2007) 313–316.
[36] M. Zaiser, J. Schwerdtfeger, A.S. Schneider, C.P. Frick, B.G. Clark, P.A. Gruber, E. Arzt, Strain burts in plastically deforming molybdenum micro- and nanopillars, Phil. Mag. 88 (2008) 3861–3874.
[37] A. Rinaldi, P. Peralta, C. Friesen, K. Sidradzki, Sample-size effects in the yield behavior of nanocrystalline nickel, Acta Mater. 56 (2008) 511–517.
[38] P.D. Ispánovitya, Á. Hegyia, I. Gromaa, G. Györgyia, K. Rattera, D. Weygand, Average yielding and weakest link statistics in micron-scale plasticity, Acta Mater. 61 (2013) 6234–6245.
[39] W. Weibull, A statistical distribution function of wide applicability, J. Appl. Mech. 18 (1951) 293–297.
[40] B. Lawn, Fracture of Brittle Solids, second ed., Cambridge University Press, 1993.
[41] U. Ramamurty, F.W. Zok, F.A. Leckie, H.E. Deve, Strength variability in alumina fiber-reinforced aluminum matrix composites, Acta Mater. 45 (1997) 4603–4613.
[42] J.C.M. Li, Y.T. Chou, The role of dislocations in the flow stress grain size relationships, Metall. Mater. Trans. B 1 (1970) 1145–1159.
[43] G.T. Gray, T.C. Lowe, C.M. Cady, R.Z. Valiev, I.V. Aleksandrov, Influence of strain rate & temperature on the mechanical response of ultrafine-grained Cu, Ni, and Al-4Cu-0.5Zr, Nanostruct. Mater. 9 (1997) 477–480.
[44] Y.M. Wang, E. Ma, Three strategies to achieve uniform tensile deformation in a nanostructured metal, Acta Mater. 52 (2004) 1699–1709.
[45] Z.X. Wu, Y.W. Zhang, M.H. Jhon, J.R. Greer, D.J. Srolovitz, Nanostructure and surface effects on yield in Cu nanowires, Acta Mater. 61 (2013) 1831–1842.
[46] P.M. Derlet, H.V. Swygenhoven, The role played by two parallel free surfaces in the deformation mechanism of nanocrystalline metals: a molecular dynamics simulation, Phil. Mag. A 82 (2002) 1–15.
[47] D.S. Gianola, D. Farkas, M. Gamarra, M. He, The role of confinement on stress-driven grain boundary motion in nanocrystalline aluminum thin films, J. Appl. Phys. 112 (2012) 124313.
[48] S. Agepati, P. Ghosh, A.H. Chokshi, Microstructural evolution and strength variability in microwires, Mater. Sci. Eng. A 652 (2016) 239–249.
[49] G.E. Dieter, Mechanical Metallurgy, McGraw-Hill, London, 1988.
[50] X. Li, Y. Wei, W. Yang, H. Gao, Competing grain-boundary- and dislocation mediated mechanism in plastic strain recovery in nanocrystalline aluminum, Proc. Nat. Acad. Sci. U. S. A. 106 (2009) 16108–16113.